Using Inertial Data to Enhance Image Segmentation
Knowing Camera Orientation Can Improve Segmentation of Outdoor Scenes

Osian Haines, David Bull and J. F. Burn
University of Bristol, Bristol, U.K.

Keywords: Vision Guided Locomotion, Segmentation, Image Interpretation, Scene Understanding, Inertial Sensors, Oculus Rift, Mobile Robotics.

Abstract: In the context of semantic image segmentation, we show that knowledge of world-centric camera orientation (from an inertial sensor) can be used to improve classification accuracy. This works because certain structural classes (such as the ground) tend to appear in certain positions relative to the viewer. We show that orientation information is useful in conjunction with typical image-based features, and that fusing the two results in substantially better classification accuracy than either alone – we observed an increase from 61% to 71% classification accuracy, over the six classes in our test set, when orientation information was added. The method is applied to segmentation using both points and lines, and we also show that combining points with lines further improves accuracy. This work is done towards our intended goal of visually guided locomotion for either an autonomous robot or human.

1 INTRODUCTION

Locomotion is fundamental to the survival of humans and most other land-dwelling animals, in order to find food, escape danger, or find mates, for example. One of the primary senses used to guide locomotion is vision, enabling animals to perform complex tasks such as avoiding obstacles, route planning, adjusting to different terrains and building cognitive maps (Patla, 1997), which would be impossible with other senses. This has inspired many applications in computer vision and robotics, which also attempt to use vision to guide vehicles – either wheeled or legged – over rough terrain using visual sensors (see for example (DeSouza and Kak, 2002; Lorch et al., 2002)).

However, another sense available to animals is from the vestibular system, allowing both relative acceleration and absolute orientation (with respect to gravity) to be perceived (Angelaki and Cullen, 2008). This is combined with other senses, such as vision, and is essential for the accurate balance required for more agile motions. Interestingly, it has been suggested that the central nervous system dynamically controls the relative importance of visual and vestibular signals (Deshpande and Patla, 2007), and that vestibular sensing may have a larger effect when vision is impaired. Vestibular sensing is also able to ameliorate effects due to head motion when fixating on an object (Virre, 1996), and its absence causes severe problems in interpreting visual information.

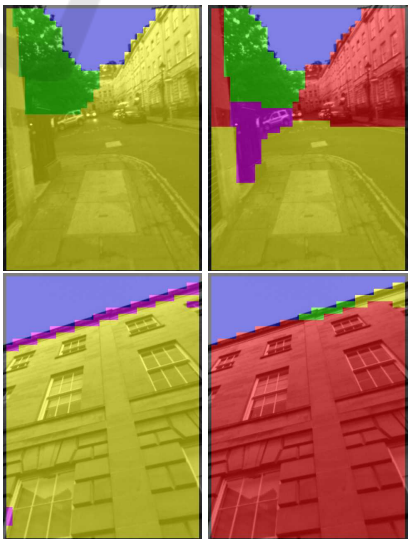

Figure 1: Typical results of our algorithm, showing how segmentation results using only vision (left) can be improved by taking into account the camera orientation (right). In both examples knowledge of the camera orientation avoids misclassifying vertical walls as ground (yellow). See Fig. 7 for full colour legend. All images are best viewed in colour.

The use of orientation information in interpreting scene content has been less well studied in the context

Haines O., Bull D. and Burn J..
Using Inertial Data to Enhance Image Segmentation - Knowing Camera Orientation Can Improve Segmentation of Outdoor Scenes.
DOI: 10.5220/0005274000210032
In *Proceedings of the 10th International Conference on Computer Vision Theory and Applications* (VISAPP-2015), pages 21-32
ISBN: 978-989-758-090-1

of mobile robotics however, and is something which we believe can be put to good use alongside vision. This is based on the observation that different types of surface or structure are more likely to be observed when the camera is facing in different directions: for example, a camera pointing straight ahead is unlikely to see the ground in the top half of the image; or a camera pointing straight downward is very unlikely to be looking at the sky.

In this paper we show that by using information about the real-world orientation of a camera obtained from an inertial sensor, it is possible to improve the performance of algorithms designed to segment images into distinct semantic/structural regions, with the aim of facilitating autonomous navigation through urban environments – see for example Fig. 1.

While vision is a suitable sensing modality for such tasks, most solutions focus on using only visual features. While the location of a point/region in an image has previously been used to alter likelihood of predicting certain geometric classes (Hoiem et al., 2007), to our knowledge the orientation of the camera itself has not been used to facilitate segmentation in this way.

Visual navigation is an important topic in robotics, where the ability to navigate through unknown environments without human guidance is essential for tasks such as disaster relief and search-and-rescue (Kleiner and Dornhege, 2007), planetary exploration (Maimone et al., 2007), or for self-driving cars (Dahlkamp et al., 2006).

On the other hand, algorithms such as ours have the potential to be used to guide humans, as we explore in this work. We do this primarily because a human makes a convenient test-bed for evaluating vision guidance algorithms without the constraints of robot locomotor capability, and give a useful proxy for how well robots might be guided. Moreover, such algorithms could also be applicatied as navigation aids for the visually impaired, where recovering the structure of a scene is important (Brock and Kristensson, 2013; Tapu et al., 2013). This paper uses as an example the goal of designing an algorithm able to guide a human through an urban environment while wearing a head-mounted display, through which the result of our segmentation is shown.

The next section discusses related work in the field. A brief overview of our method is given in Section 3, followed by Section 4 which describes the data acquisition process. Section 5 gives full details of how our algorithm works. We then present extensive results and examples in Section 6, before concluding in Section 7.

2 RELATED WORK

Combining inertial sensors with computer vision algorithms has been known to improve performance in a variety of tasks. One of these is visual simultaneous localisation and mapping, in which the pose of a camera with respect to a map, and the unknown map itself, must be recovered while it is being traversed. Since inertial sensors provide an estimate of heading independent of that derived from the image stream, these estimates can be fused to improve robustness (Nützi et al., 2011), and help to mitigate scale drift (Piniés et al., 2007). A rather different example from (Joshi et al., 2010) uses inertial information for blur reduction, by using estimates of the camera's motion derived from inertial sensor during an exposure to guide deconvolution.

More related to our application are tasks such as segmenting an image into geometrically consistent regions (Hoiem et al., 2007) and segmenting road scenes into areas which are driveable or hazardous (Sturgess et al., 2009). The former uses the position of a segment within the image as a feature during classification, so that the expectation that the sky is near the top of the image, for example, is learnt from data – although in this work the camera is assumed to be in an upright position with no roll. (Sturgess et al., 2009) and more recently (Kundu et al., 2014) show interesting examples of combining visual segmentation with 3D information, which respectively use features extracted from a point cloud to help classify objects in road scenes, and fuse 2D segmentations and point clouds to semantically label structure in 3D. While the orientation of the camera may effect the result via the 3D map, this is not directly investigated, and furthermore is estimated from the image stream itself. Use of 3D information in the form of depth data is also useful in semantic segmentation (Gupta et al., 2014).

The use of inertial data for terrain classification was investigated by (Sadhukhan et al., 2004). Rather than use knowledge of gaze direction to guide segmentation, the inertial data themselves are used as features to encode the vehicle vibration and accelerations for different terrains, in order to predict the terrain type which the vehicle is currently traversing.

While these show interesting uses of information not directly present in the image to aid labelling, they are not making use of the information potentially provided by the camera orientation itself. Similarly, while some of the above mentioned works use inertial data to aid vision tasks, this is generally in a purely geometric sense, and they have not exploited the relevance to semantic attributes in the image. We investigate ways to do this in the following sections.

3 OVERVIEW

In this paper we present an algorithm able to take a single image with associated 3D orientation, measured with an inertial measurement unit (IMU), as input, and produce a segmentation of the image into distinct regions, corresponding to classes relevant to the task of locomotion. The classes used are: ground (walkable), plane (non-walkable, usually vertical), obstacle (non-walkable and not planar), stairs, foliage, and sky (coloured yellow, red, magenta, cyan, green and blue respectively in all examples). These were chosen as a reasonably minimal set of necessary classes to facilitate locomotion through different environments. The reason we use more than two classes (simply walkable/non-walkable) is to give more information to the human (or equivalently, robot) being guided – for example, stairs can be traversed, but with caution; foliage may be walkable but may require a different gait; and a sky region should be interpreted very differently from an impending obstacle, despite the fact neither facilitate locomotion. Of course, our algorithm is not specific to the classes we use.

To demonstrate the use of orientation in enhancing segmentation, we developed a relatively simple means of classifying and segmenting images. We segment each image by describing a grid of points with a collection of feature vectors, comprised of visual and orientation information. These are used to predict the most likely class for the point, using a pre-trained classifier. Since each point is classified independently, this initial segmentation exhibits much noise. To mitigate this, we use a Markov random field algorithm to enforce the assumption of smoothness. With this framework we show that fusing visual and orientation information can substantially improve segmentation accuracy over using either alone.

We also show that using both visual and orientation features improves performance when classifying lines in the image. As above, these are described with a combination of vision and orientation features, plus features encoding some properties of the line itself. Finally, we show that combining the results from both point and line classification can improve performance over either in isolation.

The result of our method is a segmentation of the image, comprised of sets of contiguous points with the same classification. This is not a per-pixel segmentation, due to the resolution of the grid we use, but every pixel in the image is covered, and every pixel is used for the description. As shown in Fig. 1, this is able to divide the image into regions appropriate for a navigation task.

4 DATA ACQUISITION

To develop and evaluate the algorithms in this paper, we gathered long video sequences (totalling around 90 minutes of footage) using an IDS uEye USB 2.0 camera[1] fitted with a wide-angle lens (approximately 80° field of view). This provides images at a resolution of 640×480, at a rate of 30 Hz.

Our aim is to use this method to guide humans through outdoor environments. Therefore, all our data are gathered from a camera mounted on the front of a virtual reality headset, worn by a person traversing various urban environments. While walking, the subject sees only the view through the camera. This was done so that the data are as close as possible to what would be observed in a real application – both in terms of height from the ground and viewing angle, but also the typical movements and gaze directions made by a person wearing such a headset, with somewhat limited visibility.

The hardware we used for this was the Oculus Rift[2] (Dev. Kit 1), which has a large field of view and sufficiently high framerate (up to 60 Hz). The camera was mounted sideways, so that the images have a portrait orientation – this is because the view for each eye is higher than it is wide. We correct for barrel distortion introduced by the lens to produce an image approximating a pinhole camera, using camera parameters obtained with the OpenCV calibration tool.[3]

To gather orientation information we used the inertial sensor built into the Oculus Rift. This comprises a three-axis accelerometer, gyroscope and magnetometer, which are combined with a sensor fusion algorithm to give estimates of orientation in a world coordinate frame at 1000 Hz. We retrieve the orientation as three Euler angles, and discard the yaw angle (rotation about the vertical axis), since in general this will not have any relationship to semantic aspects of the world. Conversely, pitch and roll are important since they encode the camera pose with respect to the horizon line, and thus whether the camera is looking up/down or is tilted. This has an influence on the likelihood of different classes being observed.

From these videos, a subset of frames are chosen manually for labelling, either for training/validation or testing. They are divided into disjoint regions, built from straight-line segments. Each region is assigned a ground truth label from our set of classes. This is by nature a subjective task, since image content is often ambiguous, but the labelling is as consistent as possible. Some truly ambiguous regions are not labelled,

[1] en.ids-imaging.com
[2] www.oculus.com
[3] www.docs.opencv.org

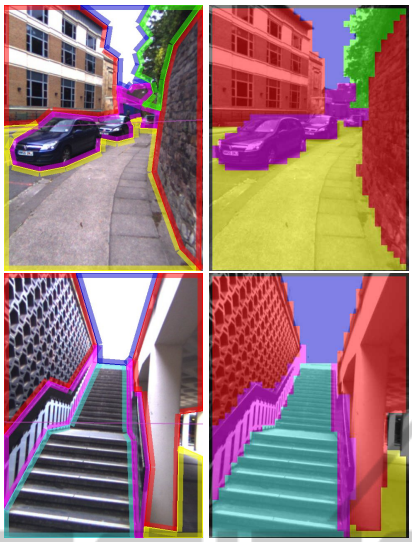

Figure 2: Example ground truth – the manual labelling of regions (left) and ground truth segmentation (right).

which are omitted from all training and testing.

Examples of ground truth data can be seen in Fig. 2. The labelling is independent of the points and lines which are later created in the image. We also show ground truth segmentations derived from these, in which a grid of points has been assigned labels according to the the underlying ground truth (where the blockiness due to the grid is clearly visible). This is the best possible segmentation, against which we evaluate our algorithms in Section 6.

5 CLASSIFICATION AND SEGMENTATION

In this section we describe the process by which an image is segmented, according to either the visual features, orientation features, or both; and where these features are created in regions surrounding grid points, detected lines, or both. An overview of the whole system is presented in Fig. 3.

5.1 Features

To describe a point, we build feature vectors from the pixels in a square patch surrounding the point. We use two types of visual feature: histograms of gradients, and colour histograms.

Histograms of gradients are used to represent the texture of the patch. The image is convolved with gradient filters in the x and y directions, to obtain at each pixel gradient responses g_x and g_y. For each pixel in a patch we calculate $\theta = tan^{-1}\frac{g_y}{g_x}$ and $m = \sqrt{g_x^2 + g_y^2}$, which are the gradient angle and magnitude respectively. These are used to build the gradient histogram by quantising the angle into bins, and weighting the contribution to each bin by the magnitude. Rather than creating a single orientation histogram for each patch, we follow the example of (Haines and Calway, 2012) and create four separate histograms for each quadrant of the patch, and concatenate them together in order to encode richer structure information. This is similar to the way HOG descriptors are built from multiple cells (Dalal and Triggs, 2005), but without the overlapping blocks.

Colour has also been shown to be beneficial when classifying and segmenting images (Hoiem et al., 2007; Krähenbühl and Koltun, 2011). The colour features we use are histograms built in HSV space, which combine a histogram of quantised hue values, weighted by the saturation (since the saturation represents the degree to which the hue is relevant), and a separate histogram of the intensity values, to encode the distribution of brightnesses within the patch.

We shall henceforth refer to the above as 'vision features'. The other type of features are the 'orientation features'. To compute these, we use the pitch and roll values from the Oculus Rift IMU, each normalised to the range $[0,1]$. In addition to these, the feature vector contains the position in the image of the point (normalised by the image size). This is important, since otherwise the orientation feature would be the same for all points in the image: it is the interaction between image position and camera orientation which gives rise to cues of different types of structure at different locations in the image.

5.2 Line Regions

An alternative form of the algorithm uses a set of lines detected in the image. This is done in order to represent high-frequency image content, and distinctive texture and colour occurring over discontinuities, which would be missed by the much smaller point features. To detect lines we use the LSD line segment detector[4] (Von Gioi et al., 2010). The regions are created around these lines, extending along their length and covering a region of fixed width on either side (we discard lines under 6 pixels long and 3 pixels wide (LSD gives a width value for each line) since these are likely to be noise).

Line regions too are endowed with both visual and orientation features. In order to create a description better suited to lines, for both gradient and colour we create pairs of histograms, from the pixels in rectangular regions either side of the line, and concatenate

[4]Code available at www.ipol.im/pub/art/2012/gjmr-lsd

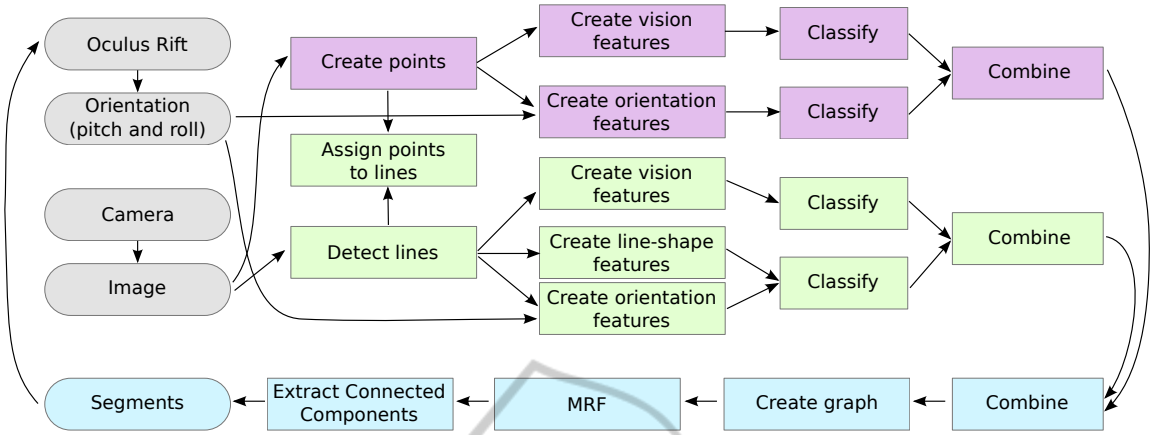

Figure 3: Block diagram showing how the system as a whole works. The different algorithms discussed in this work correspond to all or some of this. The 'combine' blocks can be interpreted as applying meta-learning, or concatenating features *before* classification, as appropriate.

them. Thus, the gradient descriptor has half the dimensionality compared to the point case, while the colour descriptor is twice as long.

We also add a line shape descriptor, which comprises simply its length, width, and orientation in the image, each appropriately normalised. Finally, we use the same orientation descriptor, using the line's midpoint and the pitch and roll of the camera as above (we will refer to these together as the orientation features unless otherwise stated). The use of these features separately and together is evaluated in Section 6.

In order to combine lines with the rest of the segmentation, we assign points to lines if they lie within the region enclosed by the line feature (a point may be assigned to multiple lines). It is this assignment of points to lines which later allows line classifications to be transferred to points for segmentation; similarly, the ground truth label of a line is obtained via the points, whose label in turn comes from the marked ground truth regions (thus a line's label vector is the mean label vector of all points inside the area used to describe it).

5.3 Classification

Having extracted features for all points and lines in our training set, each being paired with a ground truth label, we train a set of classifiers, with which we can then predict labels for points and lines in new images. For learning and prediction, we represent each label as a 1-of-K vector (for the $K = 6$ classes), where dimension k is 1 for class k, and zero otherwise. The outputs of the classifiers, after normalising to sum to 1, are treated as estimated probabilities for each class.

The classifier we use for this work is multivariate Bayesian linear regression (Bishop, 2006), chosen because it is both fast to train, and very fast to evaluate for a new input. It is similar to standard regularised linear regression, except that the optimal value for the regularisation parameter can be chosen directly, under the assumption that the data have a Gaussian distribution. Since it is multivariate regression (predicting the K dimensions of the label vector), an $M \times K$ weight matrix is learnt, for M data. Prediction with the linear regressor is simply a matter of multiplying the feature vector by the weight matrix. Rather than the raw feature vector – which would allow for learning only linear combinations of the inputs – we use fourth order polynomial basis functions.

5.4 Combining Information

We can easily run the algorithm using points (**P**) or lines (**L**) with either vision (**V**) or orientation (**O**) features in isolation. This leads to the four baseline methods (denoted **P-V**, **P-O**, **L-V** and **L-O** respectively, where L-O combines both orientation and line-shape features as discussed above). The main theme of this paper is to combine information from multiple feature types (vision/orientation) and from different image entities (points/lines), which we describe here.

When classifying points, we can combine the features in one of two ways. First and most obviously, we simply concatenate the vision and orientation features into one longer feature vector, and train/test with this (algorithm **P-VO-Cat**). Or, we train separate classifiers for the two feature types, and combine them afterwards. This is achieved by concatenating the output K-dimensional label vectors from each classifier for a point and treating this as a new feature vector. This is input to a second round of classification, the output of which is another K-d label vector, represent-

ing the final probability estimate for each class. This process is known as 'meta-learning' (or sometimes 'stacked generalisation') (Bi et al., 2008). To train the meta-classifiers, we run the classifiers whose outputs we wish to combine on all points in the training data, to gather example outputs. These predicted label vectors are concatenated (to make the 'meta-features'), and paired with the known ground truth label for each point to train the meta-learner. We refer to this algorithm as **P-VO-Meta**.

The above can also apply to line regions, i.e. we can combine line features either by concatenation or meta-classification (**L-VO-Cat** and **L-VO-Meta**). However, we cannot combine points with lines by simply concatenating their features, because the point and line features are created over different areas. Instead, we again use meta-learning, applied at the points. Each point which lies in at least one line region is assigned the mean label vector from all lines in which it lies (again normalised to sum to 1). Then a final meta-classifier is trained using the predicted features from the points and lines as inputs, to predict the final label vector assigned to the point.

There are still two ways in which this could be done, depending on how the features were combined for the entities: either we concatenate the results of P-VO-Cat and L-VO-Cat to make the meta-feature (**PL-VO-Cat**); or use meta-classifiers for everything, and concatenate the outputs of all predicted vectors from P-V, P-O, L-V and L-O into a meta-feature, which we call **PL-VO-Meta**. In either case, we need to deal with points which are not in any lines: for PL-VO-Cat we simply use the existing result of P-VO-Cat; for PL-VO-Meta we train yet another meta-classifier, which fuses the results of only P-V and P-O, i.e. fall back to P-VO-Meta (the converse is not necessary, since there are no points belonging to lines without their own classifications). The performance of all of these combinations is compared in Section 6.

5.5 Segmentation

The result of any of the above algorithms is a set of points in the image, each having a predicted label vector, from which we choose the most likely class assignment as the dimension with the highest value. Since each point is classified individually, there is no guarantee that neighbouring points will have similar labels, even if they belong to perceptually similar regions of the image; this is especially true when using line regions, as adjacent points may be assigned to different lines.

To address this, we follow what has become fairly standard practice in such tasks (Delong et al., 2012) and formulate the problem as a Markov random field (MRF). This allows us to choose the best label for each point according to its observation (i.e. classification result), while also incorporating a smoothness constraint imposed by its neighbours.

We create a graph connecting all the points in the image – this is simply a grid connecting a point to its 4-neighbours. The aim when optimising a MRF is to maximise the probability of the configuration of the field (i.e. an assignment of labels to points); this is equivalent to minimising an energy function over all cliques in the graph (Li, 2009). We define the neighbourhood to include up to second-order cliques, i.e. unary and pairwise terms.

A configuration of the MRF is represented as $p = (p_1 ... p_N)$, where $p_i \in \mathcal{L}$ is the class assigned to point i of N and $\mathcal{L}$ is the set of possible labels. The goal is to find the optimal configuration p^*, such that $p^* = \mathsf{argmin}_p E(p)$, where $E(p)$ is the posterior energy of the MRF. We define this as:

$$E(p) = \alpha \sum_{i=1}^{N} \psi_d(p_i) + \sum_{i=1}^{P} \sum_{j \in \mathcal{N}_i} \psi_s(p_i, p_j) \quad (1)$$

where the first term sums over all points in the graph, and the second sums over all neighbours $\mathcal{N}_i$ for each point i. α is a weight parameter, trading off the effects of the data and the smoothness constraints. The unary and pairwise potentials are:

$$\begin{aligned} \psi_d(p_i) &= \|\mathbf{p}_i - \mathbf{c}_i\| \\ \psi_s(p_i, p_j) &= V_{ij} T(p_i \neq p_j) \end{aligned} \quad (2)$$

Here, $\mathbf{p}_i$ denotes the label p_i represented as a 1-of-K vector, and $\mathbf{c}_i$ is the K-d output of the classifier. The Euclidean distance means the predicted probability for all the labels is taken into account. $T(.)$ is an indicator function, returning 1 iff its argument is true, and V_{ij} is a pairwise interaction term, controlling the degree to which label dissimilarity is penalised at sites i and j. This is set to $V_{ij} = \beta - \mathsf{min}(\beta, |m_i - m_j|)$, where m_i is the median intensity over the patch at point i. This penalises differences in label more strongly between points with similar appearance, in order to adapt the segmentation to the underlying image contours. We set the parameters to $\alpha = 60$ and $\beta = 90$ empirically based on observations on the training set (note the pixel intensities are in the range $[0, 255]$). We optimise the MRF using graph cuts with alpha-expansion[5] (Delong et al., 2012).

Once the MRF has been optimised, each point has one label, and points with the same label should be spatially grouped together. To extract the final segments, we perform connected component analysis, so one segment is created for each contiguous graph component with the same label.

[5]Using the 'gco-v3.0' code at vision.csd.uwo.ca/code

6 RESULTS

To evaluate our algorithms, we gathered two datasets in the manner described in Section 4. All data were obtained from the same camera, having a (rotated) resolution of 480×640, and were corrected for barrel distortion due to a wide-angle lens.

The first dataset was designated the training set, and contained 178 manually labelled images. This set was used for cross-validation experiments, to demonstrate the claims made above. The second set of 156 images was the test set – this was obtained from different video sequences, from physically distinct locations to the training set to ensure there was no overlap during training and testing. This was done to verify that the algorithms generalise beyond the training set, and to show example images (all examples in the paper come from this set). All our labelled data are available online.[6]

Our algorithm has a large number of parameters which will effect its operation. The most important ones are described here, with typical values given. The grid density (distance between points) was set to a value of 15 pixels (making a grid of approximately 30×40 points), to give a compromise between an overly coarse representation/segmentation, and the quadratic increase in computational time for denser grids. The patches around every pixel, from which visual features are built, were squares of side 20 pixels. The width of line regions was set to 30. The basic gradient histogram was 12-d, making the concatenated quadrant feature on points 48-d; and HSV histograms had 20 dimensions each for the hue and intensity parts. As described earlier, point-orientation features had four dimensions, while lines had those four, plus the three for line shape.

These parameters were set to values which appear sensible or are supported by related literature. However, we make no claim that these were the optimal parameters, and much further tuning could be done, although the best settings would depend on the dataset used. We emphasise that this does not alter the central claims of this work, i.e. that making use of orientation information, using either points or lines, can improve segmentation. All parameters were kept constant across evaluations, so all results are relative.

6.1 Cross-validation

We begin with results obtained through cross-validation on our training set. This was done by running five independent runs of five-fold cross-validation on the data (to mitigate artefacts due to particular choices of training/test splits). We use classification accuracy as our error measure, i.e. the average number of times a point was assigned the correct class (we also looked at the diagonal of the confusion matrix, or the mean of F-measures over all classes, and observed the same trends). We evaluated segmentation point-wise, i.e. looking at every point individually, since for the time being we are not concerned with the issue of true segments being wrongly split or merged. For this reason, and because it may mask some of the differences between algorithms, all evaluations were performed without using the MRF segmentation; instead we directly used the labels assigned to points by the classifiers (we found the MRF generally improved accuracy by a few percent).

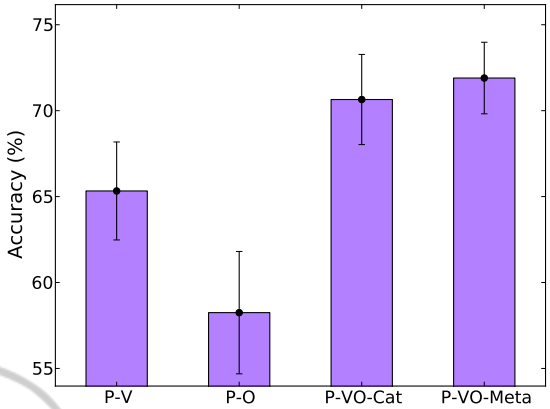

Figure 4: Adding orientation features to vision features for points. All error bars show a 95% confidence interval.

First, we ran an experiment to compare classification using only points, with vision features (P-V) or orientation features (P-O) only, and combinations of the two. The results are shown in Fig. 4. The bars indicate the average accuracy over all the runs of cross-validation, and the error bars are drawn to show a 95% confidence interval, based on the average standard error over all runs of cross-validation.

As one might expect, using only orientation features performs much worse than using only vision, since it is utterly unable to predict foliage, for example. Nevertheless, it can be surprising what orientation alone can tell us about what an image is expected to contain, as we will show in the next section.

One of the key results of this paper is that either of the combination methods (P-VO-Cat, P-VO-Meta) are clearly better than either vision or orientation features alone. It is interesting to note that classifying separately followed by meta-learning improves performance somewhat (consistently albeit perhaps not significantly). This may be because it is able to learn interactions between the classifiers not apparent when

[6]Out dataset can be found at www.cs.bris.ac.uk/~haines

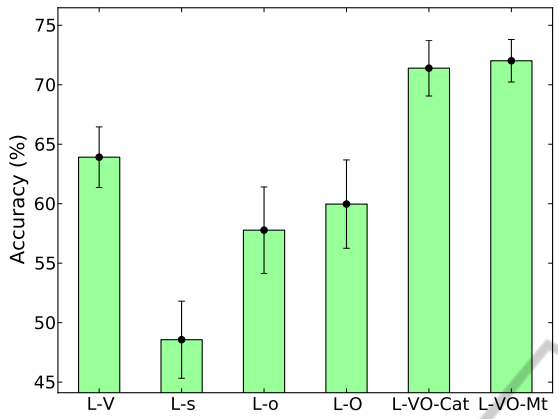

Figure 5: Using orientation with vision features for lines. L-s and L-o respectively denote shape and orientation features individually, and L-O concatenates both.

only one long feature vector is used; or because a 4-d orientation vector added to a 88-d vision feature has difficulty making a large difference. However, we cannot exclude the possibility that this is a consequence of our choice of classifier.

The next experiment was the same as the above, but for line regions instead. Note that these evaluations were done using the points which were assigned labels from classified lines, not on the lines themselves (points not in lines were excluded from the evaluation). We also tested the use of orientation (**L-o**) and shape (**L-s**) features separately, then together (L-O), showing that knowledge of the lines' size and orientation in the image, combined with the camera orientation, is better than using the camera orientation alone. As Fig. 5 shows, the same trend as in the points experiment is observed: orientation and shape alone (L-O) cannot compete with vision only (L-V), but once again combination by concatenation (L-VO-Cat) or meta-classification (L-VO-Meta) improve performance (the latter two, like V-O, concatenate the shape features with the orientation)

Finally, we investigated the effect of combining point and line features. Figure 6 shows both point and lines separately, using both types of feature (we show the individual meta-classifier versions because they are better; points and lines appear to perform similarly, though note that the lines were evaluated at only a subset of points). The two methods of combining entities (PL-VO-Cat and PL-VO-Meta) lead to an improved accuracy, suggesting that combining information from multiple types of patch/region is indeed beneficial, albeit by a smaller margin than the above experiments. Strangely, the best performance is achieved by PL-VO-Cat, which concatenates the result of the less-good concatenation versions of the individual entities, though the difference is small.

In Fig. 7 we show a confusion matrix, obtained as the mean confusion matrix over all runs of cross-validation, for PL-VO-Cat, the best performing variant. The diagonal is pleasingly prominent, though there is significant confusion between stairs and ground (when the true class is stairs), which is somewhat unfortunate from a safety point of view. Vertical surfaces also tend to be confused with other obstacles and foliage, which is less of a concern. For our task, ground identification is perhaps the most important criterion, which appears to be the strongest result.

6.2 Independent Data and Examples

After the cross-validation experiments, we trained sets of (meta-)classifiers corresponding to different variants of the algorithm, using the training set above (plus copies obtained by reflecting across the vertical image axis). We used these to evaluate performance on the independent test set. Results are shown in Table 1. This confirms the important result of the paper: that combining orientation information is beneficial, exhibiting around 10% increase in overall accuracy. Adding line information did confer a further improvement, although this was only slight. We also show results after applying the MRF, which increased accuracy by a few percent in each case.

We now show example results taken from the test set, showcasing the differences between the algorithms presented above. These images were chosen to be representative examples of what the algorithms can achieve, and where applicable, we choose the -Cat or -Meta versions which gave the best performance in the tests above. In all example images in the paper, the MRF segmentation has been run, to remove noise and give a tidier segmentation.

First, Fig. 8 shows side by side examples of the

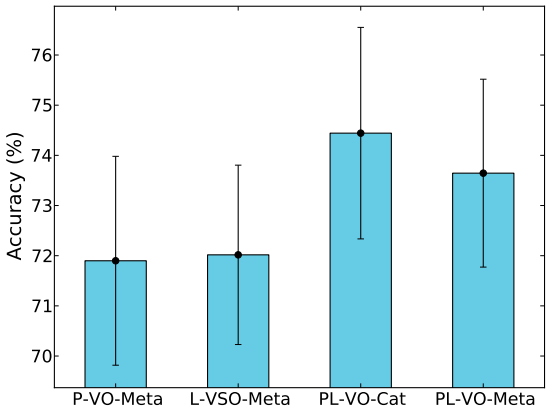

Figure 6: Combining predictions from both points and lines.

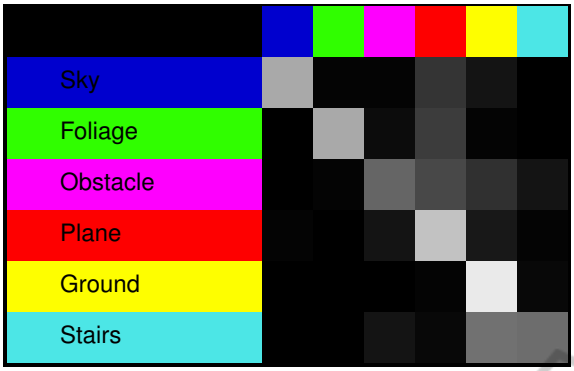

Figure 7: Confusion matrix over all runs of cross-validation, for the best-performing algorithm PL-VO-Cat. Rows correspond to the true classes, while columns represent the predicted classes. Colours correspond to those used through all segmentation examples.

basic vision version (P-V), and the effect of adding orientation (P-VO-Meta). In the top example, the building façade is partly mistaken for the ground by the visual features, whereas knowing the camera is pointing upwards corrects this. In the bottom example, the mis-classification of the road as stairs is also corrected.

In the next example (Fig. 9) we show the effect of adding line classifications to the points-only segmentation, in both cases using both visual and orientation features (P-VO-Meta, PL-VO-Cat, respectively). These examples show how the information gleaned from the lines can aid segmentation, for example by disambiguating stairs and planes, or finding non-planar objects. However, as our results below will show, lines can sometimes be detrimental.

It is interesting to see what effect the orientation features have, independently of the vision features, so in Fig. 10 we show results generated using P-O and PL-O, i.e. there are no visual features at all being used in these segmentations (image information is being used only for line detection). Figure 10(a) appears to be correctly segmented, but only because this is a common and rather empty configuration of ground and walls; whereas the cars in (b) are obviously ignored. (c) is interesting since it shows that with the camera looking down at a certain angle, stairs

Table 1: Comparison of the different algorithms on independent test data. Using a MRF to smooth away spurious local detections increases accuracy slightly in all cases.

Algorithm	Accuracy	With MRF
P-V	61.0%	64.7 %
P-VO	71.1%	73.8 %
PL-VO-Cat	71.5%	74.6 %
PL-VO-Meta	72.0%	74.3 %

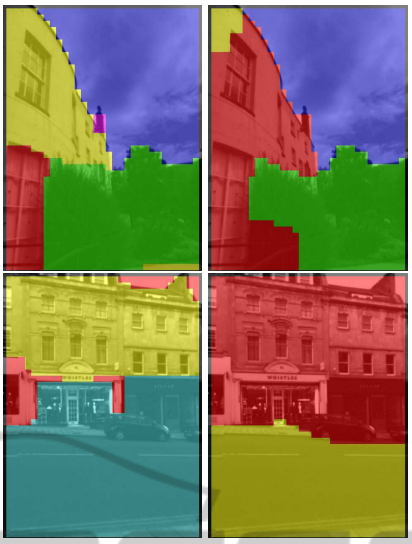

Figure 8: Example results, showing segmentation using only vision features (left) and combined with orientation features in (right). See colour legend in Fig. 7.

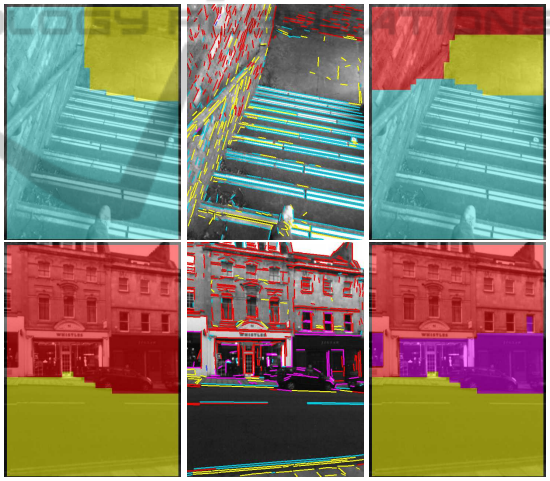

Figure 9: Examples showing how adding line classifications (centre) in conjunction with point features (P-VO-Meta, left) can help improve segmentation results (PL-VO-Cat, right).

are predicted – in this case correctly. This raises the interesting issue that stairs are predicted here not just because they are likely to be below the viewer, but because the viewer is likely to look downward when walking up stairs. In 10(d) and (e) the use of lines has altered the segmentation, to give the impression it is seeing the bollards and the sky (the points assume there is sky above, but lines even at such a height are rarely labelled as sky in the training set). In (f) the lines themselves are shown, and it can be seen how their orientation in the image has an effect, since the bollards and paving stones are classified differently, despite being at around the same image height.

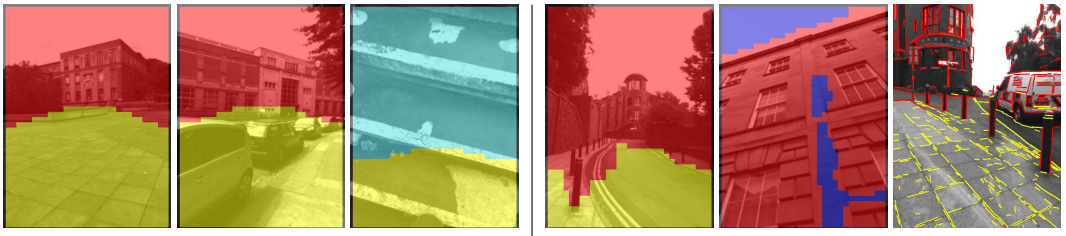

(a) (b) (c) (d) (e) (f)

Figure 10: Example segmentations using only orientation information features – points only (a-c) and points with lines (d-f). (f) shows the lines themselves, showing the effect of the lines' orientations within the image, aiding detection of vertical posts.

More examples are shown in Fig. 11. Here, we show the input image for clarity, plus the ground truth segmentation which we are aiming for. The contributions from vision (P-V), orientation (P-VO-Meta), and lines (L-VO) to the final segmentation (PL-VO-Cat) are shown. Figures 11(a) and 11(b) again show orientation information being used to improve classifications, the latter being an interesting example where adding lines improves segmentation even in the presence of motion blur. Note that the different orientations of the camera, such as in (c) and (d), mean that using only position in the image as a prior would fail.

The segmentation in Fig. 11(e) also benefits from classification of lines along the steps. Similarly in Fig. 11(c) lines help in correctly identifying the step-edges, but the step faces are classified as ground. In a way this is correct, since stairs are made up of periodic walkable regions, but this result would be marked mostly incorrect compared to our ground truth, which is labelled at a coarser resolution. This echoes our comment in Section 4 about the world being ambiguous; but also that some regions may belong to multiple classes simultaneously at different scales.

The example in 11(g) also shows orientation information being used to correctly identify the non-ground surface; however, the addition of lines in this case degrades the result. The final two rows show examples where our augmented algorithms fail to provide any benefit. In 11(h), the initial P-V segmentation is correct, and is unchanged by the addition of orientation or lines (of course, if we could achieve perfect segmentation, no amount of prior knowledge would help). On the other hand, this illustrates why it is so important that orientation does not impose a hard constraint on surface identity: even when orientation features are added, the grass (foliage class) remains. In 11(i), none of the versions of the algorithm are able to detect either the ground plane or the foliage, perhaps due to the lower level of illumination.

Our implementation, comprising unoptimised C++ code running on a Sony Vaio laptop (Intel i5, 2.40 GHz), processes one image in 1.7 seconds on average (around 6 Hz). This is well below the camera rate, but fast enough for some real-time use, when moving at low speeds; further improvements could be made by parallelising the code or using a GPU.

7 CONCLUSION

We have presented a way of combining information about the real-world orientation of a camera, obtained through inertial measurements, with more traditional vision features, for an image segmentation algorithm. This focused on our example application of scene segmentation for locomotion in outdoor environments, but we would expect the results to be applicable to other types of classification, segmentation, scene understanding and image parsing tasks where the orientation of the camera is likely to effect the likelihood of observations. We have also shown that adding orientation information is beneficial for line regions; and that combining points and lines in a similar manner can lead to some further improvement.

In our experiments it was not our intention to show whether our method can compete with the state-of-the art in image or scene segmentation, for example (Gould et al., 2009) or (Domke, 2013). Rather, we used a comparatively basic design of segmentation algorithm to highlight the effect of using extra prior information, avoiding the complexity of advanced statistical techniques. An interesting avenue of further research however to see how orientation priors can be combined with powerful techniques such as conditional random fields (Krähenbühl and Koltun, 2011).

Other future work will look at ways to create more accurate and detailed segmentations, and to implement this in a real-time setting. It would also be interesting to combine this method with temporal information, enforcing consistency across frames; or to combine with depth or 3D data.

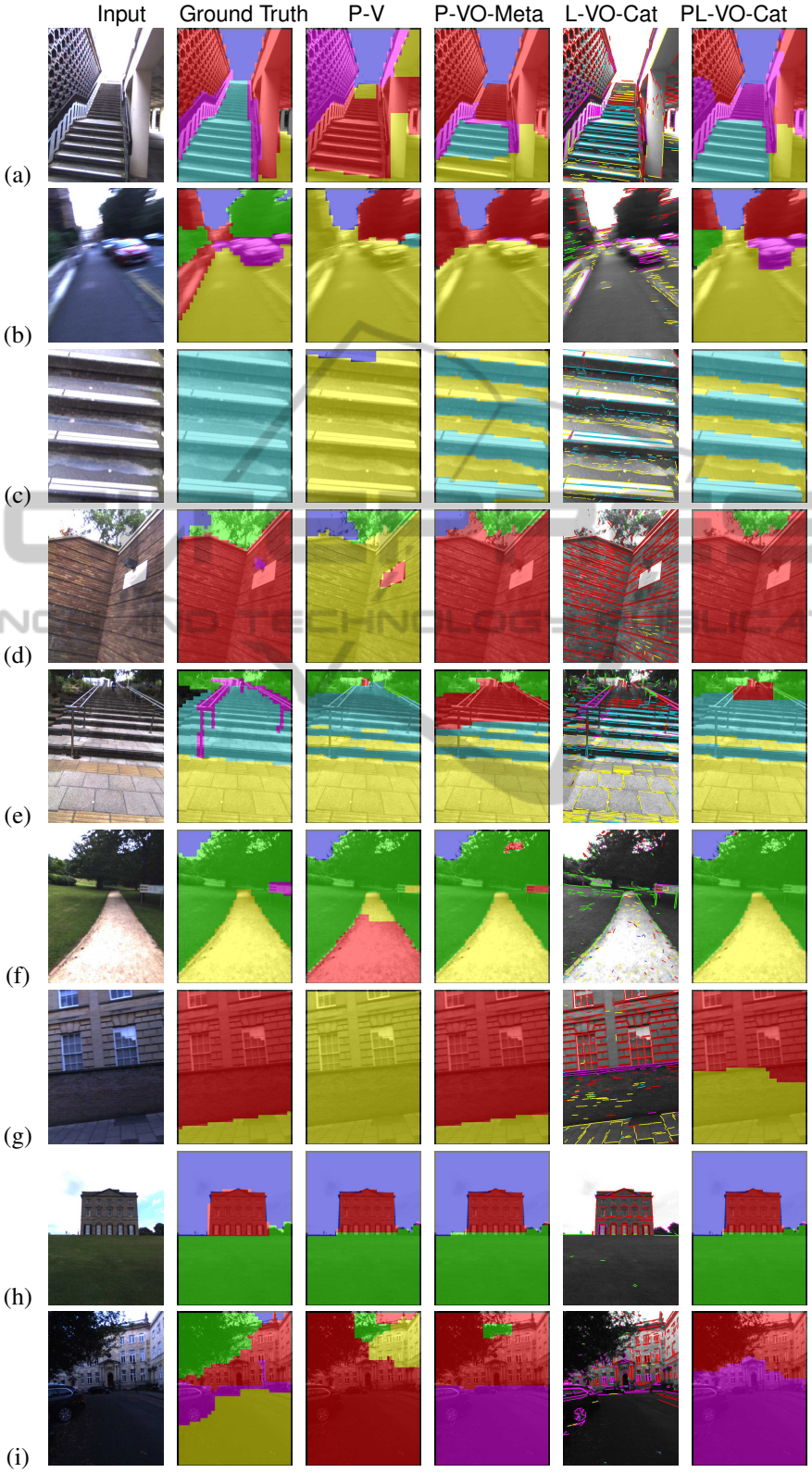

Figure 11: Example results of the various algorithms. After the input and ground truth, we show the baseline result, of points with only vision features (P-V), followed by adding orientation information (P-VO-Meta). Detected and vision-classified lines are shown, before the final result, combining everything (PL-VO-Cat).

ACKNOWLEDGEMENTS

This work was funded by the UK Engineering and Physical Sciences Research Council (EP/J012025/1). The authors would like to thank Austin Gregg-Smith for advice on hardware and graphics, and Dr David Hanwell for help with maths and text.

REFERENCES

Angelaki, D. and Cullen, K. (2008). Vestibular system: The many facets of a multimodal sense. *Annual Review of Neuroscience*, 31:125–150.

Bi, Y., Guan, J., and Bell, D. (2008). The combination of multiple classifiers using an evidential reasoning approach. *Artificial Intelligence*, 172(15):1731–1751.

Bishop, C. (2006). *Pattern Recognition and Machine Learning*. Springer.

Brock, M. and Kristensson, P. (2013). Supporting blind navigation using depth sensing and sonification. In *Proc. Conf. Pervasive and ubiquitous computing adjunct publication*.

Dahlkamp, H., Kaehler, A., Stavens, D., Thrun, S., and Bradski, G. (2006). Self-supervised monocular road detection in desert terrain. In *Proc. Robotics Science and Systems*. Philadelphia.

Dalal, N. and Triggs, B. (2005). Histograms of oriented gradients for human detection. In *Proc. IEEE Conf. Computer Vision and Pattern Recognition*.

Delong, A., Osokin, A., Isack, H. N., and Boykov, Y. (2012). Fast approximate energy minimization with label costs. *International journal of computer vision*, 96(1):1–27.

Deshpande, N. and Patla, A. (2007). Visual–vestibular interaction during goal directed locomotion: effects of aging and blurring vision. *Experimental brain research*, 176(1):43–53.

DeSouza, G. and Kak, A. (2002). Vision for mobile robot navigation: A survey. *IEEE Trans. Pattern Analysis and Machine Intelligence*, 24(2):237–267.

Domke, J. (2013). Learning graphical model parameters with approximate marginal inference. *IEEE Trans. Pattern Analysis and Machine Intelligence*, 35(10):2454.

Gould, S., Fulton, R., and Koller, D. (2009). Decomposing a scene into geometric and semantically consistent regions. In *Proc. IEEE Int. Conf. Computer Vision*.

Gupta, S., Arbeláez, P., Girshick, R., and Malik, J. (2014). Indoor scene understanding with rgb-d images: Bottom-up segmentation, object detection and semantic segmentation. *Int. Journal of Computer Vision*, pages 1–17.

Haines, O. and Calway, A. (2012). Detecting planes and estimating their orientation from a single image. In *Proc. British Machine Vision Conf.*

Hoiem, D., Efros, A., and Hebert, M. (2007). Recovering surface layout from an image. *Int. Journal of Computer Vision*, 75(1):151–172.

Joshi, N., Kang, S., Zitnick, C., and Szeliski, R. (2010). Image deblurring using inertial measurement sensors. *ACM Trans. Graphics*, 29(4):30.

Kleiner, A. and Dornhege, C. (2007). Real-time localization and elevation mapping within urban search and rescue scenarios. *Journal of Field Robotics*, 24(8-9):723–745.

Krähenbühl, P. and Koltun, V. (2011). Efficient inference in fully connected crfs with gaussian edge potentials. In *Advances in Neural Information Processing Systems*, pages 109–117.

Kundu, A., Li, Y., Dellaert, F., Li, F., and Rehg, J. (2014). Joint semantic segmentation and 3d reconstruction from monocular video. In *Proc. European Conf. Computer Vision*.

Li, S. (2009). *Markov Random Field Modeling in Image Analysis*. Springer-Verlag.

Lorch, O., Albert, A., Denk, J., Gerecke, M., Cupec, R., Seara, J., Gerth, W., and Schmidt, G. (2002). Experiments in vision-guided biped walking. In *Proc. IEEE Int. Conf. Intelligent Robots and Systems*.

Maimone, M., Cheng, Y., and Matthies, L. (2007). Two years of visual odometry on the mars exploration rovers. *Journal of Field Robotics*, 24(3):169–186.

Nützi, G., Weiss, S., Scaramuzza, D., and Siegwart, R. (2011). Fusion of imu and vision for absolute scale estimation in monocular slam. *Journal of Intelligent and Robotic Systems*, 61(1-4):287–299.

Patla, A. (1997). Understanding the roles of vision in the control of human locomotion. *Gait & Posture*, 5(1):54–69.

Piniés, P., Lupton, T., Sukkarieh, S., and Tardós, J. (2007). Inertial aiding of inverse depth slam using a monocular camera. In *Proc. IEEE Int. Conf. Robotics and Automation*.

Sadhukhan, D., Moore, C., and E., C. (2004). Terrain estimation using internal sensors. In *Proc. Int. Conf. on Robotics and Applications*.

Sturgess, P., Alahari, K., Ladicky, L., and Torr, P. (2009). Combining appearance and structure from motion features for road scene understanding. In *Proc. British Machine Vision Conf.*

Tapu, R., Mocanu, B., and Zaharia, T. (2013). A computer vision system that ensure the autonomous navigation of blind people. In *Proc. Conf. E-Health and Bioengineering*.

Virre, E. (1996). Virtual reality and the vestibular apparatus. *Engineering in Medicine and Biology Magazine*, 15(2):41–43.

Von Gioi, R., Jakubowicz, J., Morel, J., and Randall, G. (2010). Lsd: A fast line segment detector with a false detection control. *IEEE Trans. Pattern Analysis and Machine Intelligence*, 32(4):722–732.